THE JOURNAL OF PHYSICAL CHEMISTRY C
A JOURNAL OF THE AMERICAN CHEMICAL SOCIETY

pubs.acs.org/JPCC

Article

Tunable Optical Features of Graphene Quantum Dots from Edge Functionalization

Andrew Sheely, Brendan Gifford, Sergei Tretiak, and Alan Bishop*

Cite This: *J. Phys. Chem. C* 2021, 125, 9244–9252

Read Online

ACCESS | Metrics & More | Article Recommendations | Supporting Information

ABSTRACT: Graphene quantum dots (GQDs) are promising semiconducting materials for practical applications. Chemical functionalization of GQD edges is a strategy to increase their solubility and processability and to modify their optical properties. Such functionalization has a twofold effect on the electronic structure, both attributed to electronic spatial localization. The first is relevant to the introduction of electronegative species, whereas the second effect modifies the electron wave function spatial distribution through the conformational changes of geometry of the otherwise planar GQD backbone. Our computational study shows that functionalization with a weakly electronegative chlorine functional group induces small red-shifts due to the localization of excitonic states around the defect site. Groups with strong electron inducting ability such as nitro introduce stronger red-shifts. In both cases, the planar geometry of the pristine sheet is preserved when functionalization is performed at only a single site. However, functionalizing at multiple sites around the edge results in warping of the geometry of the GQD, leading to stronger electronic localizations and the largest red-shifts. This observation suggests the utility of controlling the planar geometry as a new strategy for chemically modifying 2-dimensional nanomaterials toward optical tuning.

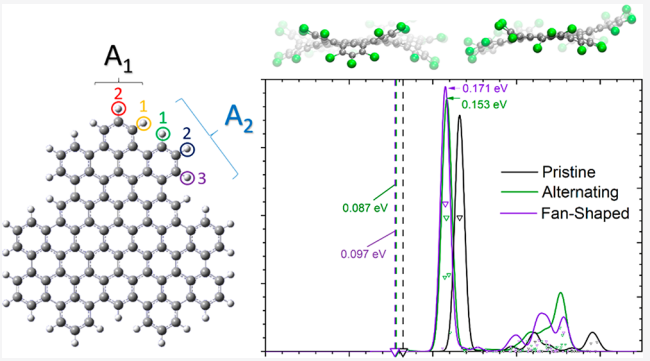

INTRODUCTION

Graphene's unique properties make it useful in a wide range of applications. As such, it has been the subject of intense study since early experimental reports.[1] The ideal structure of graphene consists of a single sheet of sp^2-hybridized carbon atoms arranged in a honeycomb-like non-Bravais lattice structure. Electronically, this creates a 2D hexagonal Brillouin zone, within which the electronic dispersion at the *k*-points is linear for an infinite sheet.[2−4] This phenomenon results in a high charge carrier mobility. In fact, the electrons and holes behave as effectively massless particles. As a consequence, graphene possesses semimetal properties. An excellent mobility of electrons in these delocalized systems makes graphene one of the most promising candidates for a new-age semiconducting material. However, the lack of a bandgap in the pristine system limits its potential uses. Owing to a very large exciton Bohr diameter, any reduction in the system size introduces the effect of quantum confinement, potentially leading to a controllable gap formation.[5] One method of introducing this confinement involves fabrication of smaller two-dimensional graphene flakes with geometrically symmetrical shapes and hydrogenated edges. When such sheets are smaller than 20 nm, they are termed "graphene quantum dots" (GQDs).[6] The finite size effects in these molecules results in a bandgap that enables their use in several types of optoelectronics technologies.[7]

In addition to opening the bandgap through finite-size effects, other methods for mitigating the limitations of the semimetal properties of bulk graphene have been developed. For instance, bottom-up synthesis of graphene-containing nanopores to enforce confinement[8] and direct observation of continuously tunable bandgaps in bilayer graphene through applied voltage[9] have been proposed. Other methods rely on functionalization (addition of chemical species through formation of sp^3-hybridized sites in a lattice of otherwise sp^2-hybridized carbon atoms). These sp^2-hybridized sites are classified as "defects", which can exist either in the central portions of the sheet or at the edges,[10] 2D analogues of topological defects on polyacetylene chains.[11] Introduction of different species at the edges of GQDs is predicted to strongly influence the emission wavelength.[12] Functionalization has recently been demonstrated as a powerful method of controlling bandgaps in graphene nanoribbons (GNRs).[13] Size-dependent effects in such systems have been controlled by the width of the sp^2-hybridized region in the GNR.[14]

Received: January 20, 2021
Revised: April 14, 2021
Published: April 27, 2021

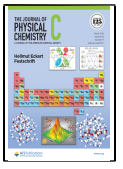

https://doi.org/10.1021/acs.jpcc.1c00537
J. Phys. Chem. C 2021, 125, 9244–9252

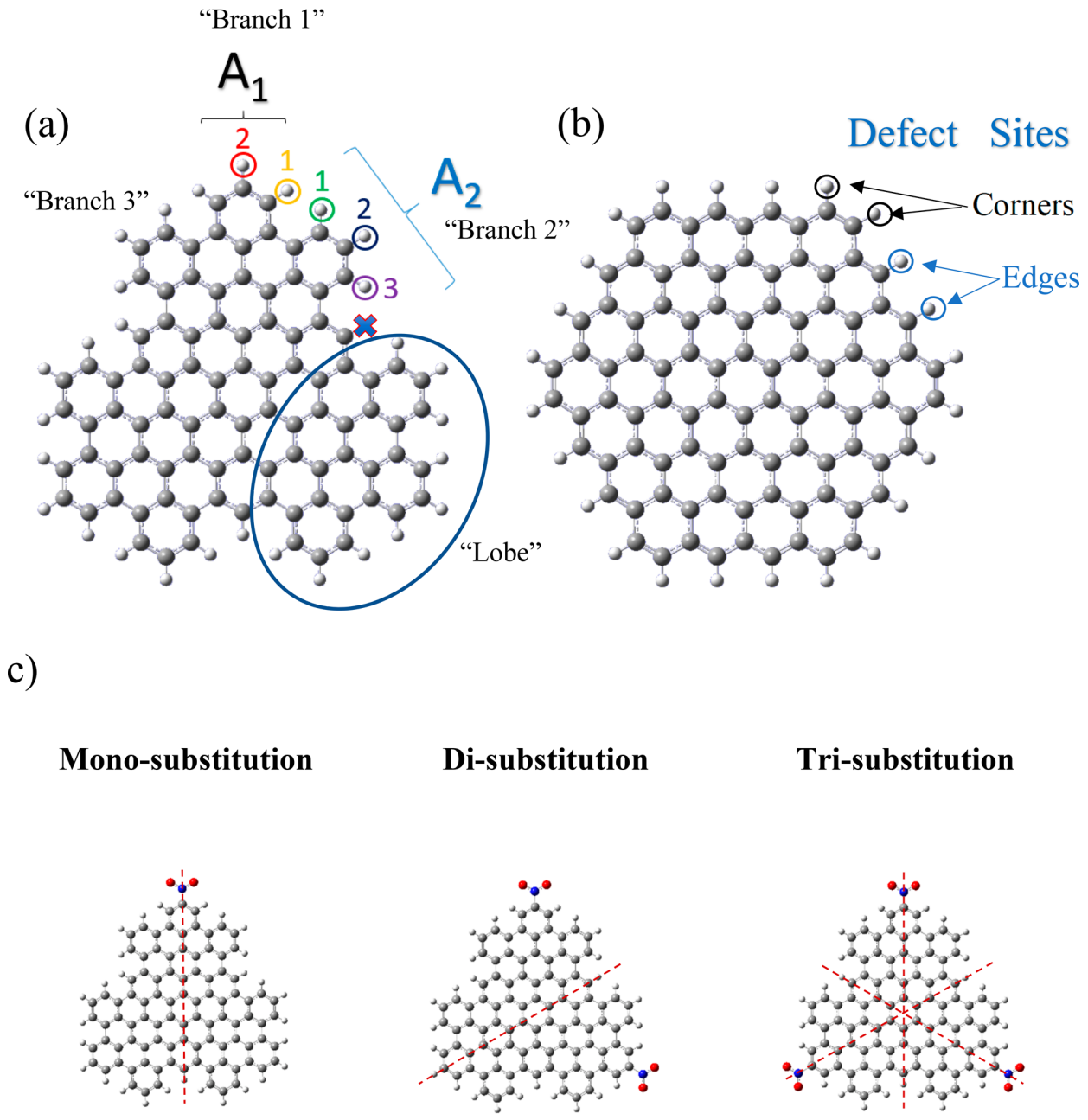

Figure 1. Selected sites for functionalization in $C_{96}T$ (a) and $C_{96}H$ (b). The positions of functionalization are notated as first the domain of the molecule (A_1, A_2) followed by the site within each domain (1, 2, 3, etc.). Thus, the sites in $C_{96}T$ are labeled as A_{12}, A_{11}, A_{21}, etc. (c) Example structures (left to right) of monosubstituted, disubstituted, and trisubstituted GQDs. The structures displayed above represent the 1-NO_2, 2-NO_2, and 3-NO_2 functionalization schemes. Symmetry lines are drawn to display the change in symmetry from one to three substitutions.

Importantly, systems of similar width but with different chemical groups at the edges have demonstrated different bandgaps. Computational results show that such variations are likely due to modification of planarity of the ribbons: GNRs with bandgaps modulated by 0.27 eV due to structural distortion from planar geometries through introduction of steric hindrance in large side groups have been engineered.[13] This indicates the potential of using such a technique in planar graphene-based nanomaterials. Markedly, GQDs are widely accessible to tuning through functionalization of the corners and edges. Instead of being terminated with hydrogen atoms (or other hydrocarbon derivatives), the edges of the graphene sheet may be functionalized with chemical reactions with a number of reagents to introduce amino, chlorine, and various other electronegative groups.[15,16] Such a strategy has even been able to produce white emission, a useful feature for light-emitting applications.[17] A traditional view is that the postsynthetic modification strongly impacts the band alignment in the electronic structure, thereby modifying the optical properties. A recent study[18] demonstrated control over the emission wavelength through functionalization of the edges of triangular GQDs with chlorine atoms. In another study, the emission color of graphene quantum dots can be tuned quite widely by chlorine doping.[19] The source of the observed red-

https://doi.org/10.1021/acs.jpcc.1c00537
J. Phys. Chem. C 2021, 125, 9244−9252

shifts remains largely unexplored. Functionalization of other graphene nanomaterials (such as single-walled carbon nanotubes) with groups of different inducting abilities[20] does not impact the optical properties nearly as drastically as reported for edge-functionalized GQDs where shifts up to 0.25 eV are observed, perhaps due to a lesser degree of quantum confinement.[18] Previous computational studies have shown that modifications of electron density around the functionalized edges of GQDs result in a perturbation to the electronic structure.[21−26] This effect was attributed to the warping of the backbone of the structure away from complete planarity. It has been previously shown that the planar structure of a pristine graphene sheet is disrupted by chlorination.[27] It is unclear whether the observed closing of the gap in GQDs with edges functionalized with chlorine is due to the effects of strictly electronic localization around the relatively electronegative chlorine atoms or a perturbation to the backbone geometry from functionalization of the edges of the otherwise planar structure.

In this work, we predict the behavior of functionalized GQDs through computations by using density functional theory (DFT) to describe the impact of functionalization on the system geometry and the consequent effects on electronic gap and optical properties. We demonstrate that the changes in electronic structure of graphene quantum dots (and therefore their optical properties) are strongly dependent on geometry changes induced by functionalization as opposed to localization of the exciton due solely to the introduction of electronegative groups. While strongly electronegative groups generate small red-shifts, the strongest red-shifts are enabled by functionalization that induces warping of the structure (i.e., strong deviation from planarity in the graphene flakes). Such deviation results in a strong electron localization, the accompanying perturbation to the frontier molecular orbitals, and the induced red-shifts. These observations suggest that efficient strategies to modify the electronic structure and resulting emission energies in these materials should account for and use geometry perturbations of the GQD, as this generates the strongest impact on the emission wavelength.

RESULTS AND DISCUSSION

Simulated GQDs Structures. Pristine experimentally relevant GQDs structures exist in two forms including trigonal ($C_{96}H_{30}$, herein termed $C_{96}T$, Figure 1a) and hexagonal ($C_{96}H_{24}$, herein termed $C_{96}H$, Figure 1b) conformations.[28] The aforementioned red-shift was experimentally observed in the $C_{96}T$ isomer.[18] Here, we explore the impact when functionalizing both of these isomers. In particular, different chemical functionalization models are considered including unfunctionalized ("pristine") GQDs, functionalization by substituting one, two, or three of the hydrogen atoms at the edge with a specific group ("monosubstitution", "disubstitution", and "trisubstitution", respectively, Figure 1c), and "fully passivated" GQDs (when every sterically accessible edge hydrogen atom is functionalized). Functionalization of $C_{96}T$ is done at five nonequivalent positions to characterize the impact on the electronic structure of functionalization of different carbon atom types as labeled in Figure 1a. The sixth distinct position is not considered due to the strong steric hindrance that would be induced by functionalization at this site.[18] These sites are then passivated with groups of differing electron-withdrawing capacity including OH, NH_2, OCH_3, CH_2, and NO_2, aiming to characterize the role of electron-withdrawing effects. Single-site functionalization of $C_{96}H$ is performed on a single edge carbon atom located along a corner. Because of symmetry, only two distinct edge sites exist for functionalization of the $C_{96}H$: in the corner and along the edge (Figure 1b). We consider the $C_{96}T$ isomer functionalized with each multiple Cl (of experimental relevance)[16] or NO_2 (which has shown to generate the strongest red-shifts). Substitutions involving difunctionalization (two groups are added in two A_{12} positions) and trifunctionalization (each equivalent position of the GQD approximately 120° apart is substituted) are constructed (see Figure 1c). Finally, a "fully functionalized" structure is explored for the $C_{96}T$ GQD decorated with chlorine atoms in all of the edge positions (except those that are highly sterically hindered, Figure 1).

Our simulation details are outlined in the Computational Methodology section. As expected, the optimized flakes retain nearly planar geometry (Figure S1). The pristine GQDs are largely conjugated systems with some rotational symmetry; C_3 in $C_{96}T$ and C_6 in $C_{96}H$. Functionalized structures (Figure 1a for $C_{96}T$ and Figure 1b for C96H) retain or lift this symmetry (Figure 1c). This enables the exploration of their optical properties through comparison of the pristine GQDs to functionalized analogues that either preserve or lift the degeneracy that is normally present. Because of symmetry, the low-energy states for the pristine $C_{96}T$ are doubly degenerate with typically one bright such as S_3/S_4 (i.e., optically allowed, high oscillator strength) and one dark such as S_1/S_2 (i.e., optically forbidden, low oscillator strength) pairs observed (Figure 2). The strongest absorption occurs through

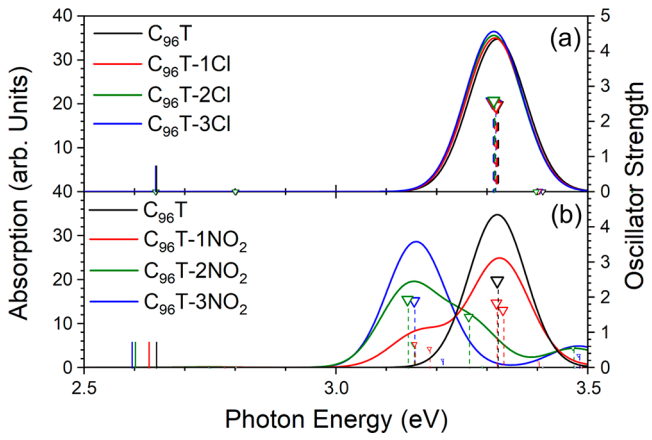

Figure 2. Calculated absorption spectra of the pristine $C_{96}T$ vs trisubstituted Cl and NO_2 GQDs. (a) Pristine C96T against mono-, di-, and trichlorinated species ($C_{96}T$-1Cl, $C_{96}T$-2Cl, and $C_{96}T$-3Cl, respectively). (b) Pristine C96T against mono-, di-, and trinitrated species ($C_{96}T$-1NO_2, $C_{96}T$-2 NO_2, and $C_{96}T$-3 NO_2, respectively). An empirical broadening line width of 0.04 eV has been used for simulating the line shape profile. Sticks indicate positions of dark states, whereas triangles display the oscillator strengths of bright transitions.

states where the transition dipoles are high, and therefore the energies of the bright states are reflective of the optical absorption energies. Because of the vibrational relaxation along the excited state potential energy surface in accordance with Kasha's rule, fluorescence energies are defined by the lowest energy transitions. We further compare how the energy of each excited state is impacted by the presence of various chemical groups. These changes in energy are then correlated to orbital

https://doi.org/10.1021/acs.jpcc.1c00537
J. Phys. Chem. C 2021, 125, 9244−9252

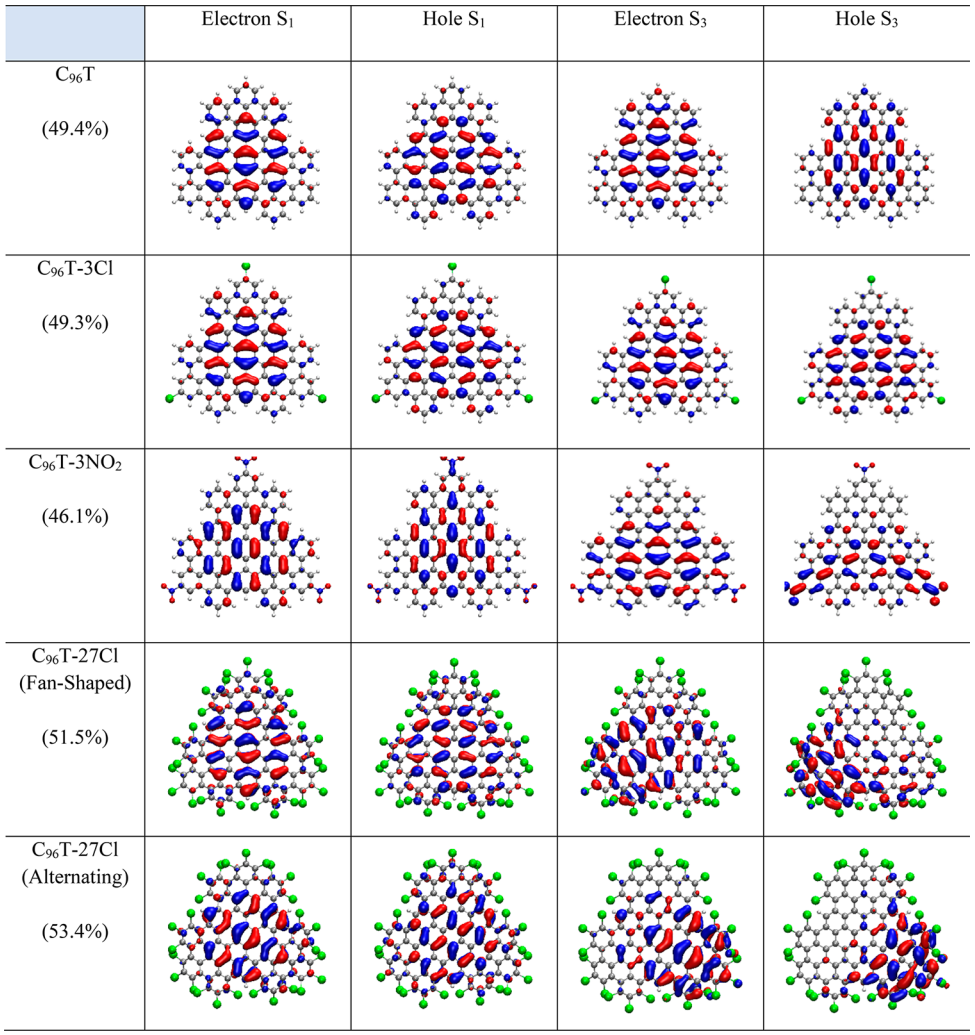

Figure 3. Natural transition orbitals of S_1 and S_3 states for selected GQD species. These transitions reflect the lowest energy and bright state, respectively. The percent contribution of each NTO pair is given in the left-hand column.

distribution of the electron density by analyzing the respective frontier molecular orbitals (FMOs) and natural transition orbitals (NTOs).

Impacts of a Single-Site Functionalization of GQDs. The precise positions and densities of functionalization in experimental systems are unknown. Therefore, the first objective of this study is to assess the impacts of functional group location on the emission wavelengths and absorption profiles for GQDs functionalized in different positions (Figure S2). Functionalization is thermodynamically favored at the A12 and A22 positions (Figure S3). This effect is likely due to the steric effects since these positions are located at "tips" of each branch corresponding with the para position on branch 1 and 2 of $C_{96}T$, respectively (Figure 1a). Therefore, substitution of the relatively small H atoms with larger functional groups is energetically more favorable in these positions. The bias toward these positions is stronger for groups that are inductively electron donating and weakest for groups that are electron withdrawing. Furthermore, marginal warping of the planar backbone is observed upon functionalization independent of the position of addition (Figure S4). This effect is strongest for bulkier methyl and methoxy groups. Because of the invariance for single-site functionalization at any site on the GQD edges, we focus on functionalizing at the A_{12} positions (for $C_{96}T$) and corners (for $C_{96}H$) for all single-site functionalizations throughout the remainder of this study.

With the exception of NO_2-functionalized structures, marginal differences are also observed for the optical properties. While CH_3, NH_2, OH, and OCH_3 minimally impact the electronic structure of the GQD (Figure S5), monosubstituted NO_2 structures result in the strongest localization effect, which can be observed in the FMOs. Functionalization with a single functional group perturbs the electronic structure and optical properties of GQDs to a degree that weakly correlates to the electron-withdrawing ability. Because of the strong inductive capacity of NO_2, it has the strongest electron localization in the FMOs, particularly the LUMO (Figure S5 for $C_{96}T$ and Figure S6 for $C_{96}H$). This behavior is pronounced in the bright states of these systems. The NTOs for monosubstituted $C_{96}T$ and $C_{96}H$ (Figure S7) both indicate the position of the exciton to be constrained close to the site of functionalization around the GQD corners. Overall, only minor impacts to geometry and electron and exciton localization are observed for all monofunctionalized species.

As far as optical energies are concerned, the most substantial impact of functionalization manifests in the splitting of the bright optical states (states S_3/S_4). It is observed that the

https://doi.org/10.1021/acs.jpcc.1c00537
J. Phys. Chem. C 2021, 125, 9244−9252

addition of a single NO_2 functionality breaks the symmetry of the originally degenerate S_3 and S_4 bright states from the pristine $C_{96}T$ and also produces two lower-bound bright states (Figure 2b, red line). A brightening of the lower-bound states in the NO_2-functionalized system is observed due to the breaking of the orbital symmetry. Functionalization of a single site with $C_{96}H$ with NO_2 produces a localization effect similar to that of $C_{96}T$, in both extent and direction (Figure S8). The remaining groups produce no significant red-shift in $C_{96}H$, as similarly shown for $C_{96}T$ structures (Figure S2). Despite the noticeable influence on localization by NO_2, the impact of functionalization with a single group has a marginal impact on the optical energies compared to other effects independent of the functional group, generating red-shifts in the bright state spanning from 0.01 to 0.223 eV. A splitting of the bright state is observed for the $C_{96}H$-NO_2 species independent of which corner site is functionalized (Figure S8). These effects lead to only small red-shifts of the main absorption state among all functionalized GQDs studied, the degree of which is closely related to the extent of electron density in the frontier molecular orbitals. Comparably smaller red-shifts are observed for the dark states, even in the case of the most inductive species (NO_2) where a red-shift of ~0.05 eV is realized. We conclude that functionalization of a GQD at a single site is insufficient to produce the significant red-shifts that are observed in experimental data.[18]

Multiple Defects. The effect of multiple functionalized sites is further explored to reveal the source of the strong experimental red-shifts by considering the $C_{96}T$ isomer terminated with Cl or NO_2 groups at all three A_{12} positions. In disubstituted structures, the symmetry of the original pristine system is broken, whereas in trisubstituted structures the symmetry is approximately retained (Figure 1c). The increase in electron-withdrawing sites results in further electronic localization from that observed in the monosubstituted structures. This trend continues with trisubstitution. In these multiple defect structures, the location and span of the exciton change from mostly centered and delocalized, as observed in the pristine $C_{96}T$ structures, to increasingly localize near the edges around the defect sites. The NTO (Figure 3) for the trichlorinated $C_{96}T$ GQD ($C_{96}T$-3Cl) displays little change from the pristine GQD; S_1 and S_3 both exhibit only minimal localization. The NTO (Figure 3) of the trinitrated GQD ($C_{96}T$-3NO_2) shows a more dramatic localization and is accompanied by a warped, nonplanar geometry. The S_1 excitation is mostly located about the center of the GQD structure and appears slightly more constrained than in the pristine case. The S_1 hole NTO appears to align with the A_{12} site preferentially. However, in S_3 the electron/hole pair is strongly localized around the lower NO_2 groups, which are bending toward the same side of the plane. The third NO_2 group (where exciton density is not found) bends toward the opposite side of the plane.

As a consequence of the nonplanarity breaking molecular symmetry and the corresponding strong exciton localization in $C_{96}T$-3NO_2, we see the predicted increase in red-shift intensity with the absorption spectra for these molecular systems (Figure 2a,b). In this case, the change in geometry plays a substantial role. Trifunctionalization results in the reemergence of state energy degeneracy in the $C_{96}T$-3NO_2 compared to the singly nitrated structures. As discussed previously, the singly nitrated $C_{96}T$ ($C_{96}T$-1NO_2) is shown to disturb the degeneracy of the excited state energies. However, functionalization on the three chemically equivalent positions does not remove this degeneracy and create new bright states below the bright S_3/S_4, but rather shifts those original bright states to a lower energy. The degeneracy is preserved due to the symmetrical functionalization, with the main changes in optical behavior resulting from the breaking of the planarity. While stronger in magnitude than for singly functionalized systems at 0.165 eV, even the strongest red-shift in the trifunctionalized case still falls short of the experimentally observed value (0.254 eV).[18] The dark states are suggestive of emission shifts that are even smaller at less than ~0.05 eV. Furthermore, the experimental results are for chloro-functionalized, for which trifunctionalization shows vanishing red-shift in our computations.[18] Despite this, the importance of changes of geometry of the planar GQD backbone on the optical properties is clear as compared to introduction of red-shifts by introducing strongly electron-withdrawing groups exclusively. Overall, these changes lift molecular symmetry constraints on the optical selection rules and lead to redistribution of the oscillator strengths across multiple states.

Higher Concentrations of Defects. We further consider the fully functionalized case of $C_{96}T$ with Cl atoms, where strong deviations from planarity are observed for the ground state geometry (Figure 4). For this triangular form, the GQD is

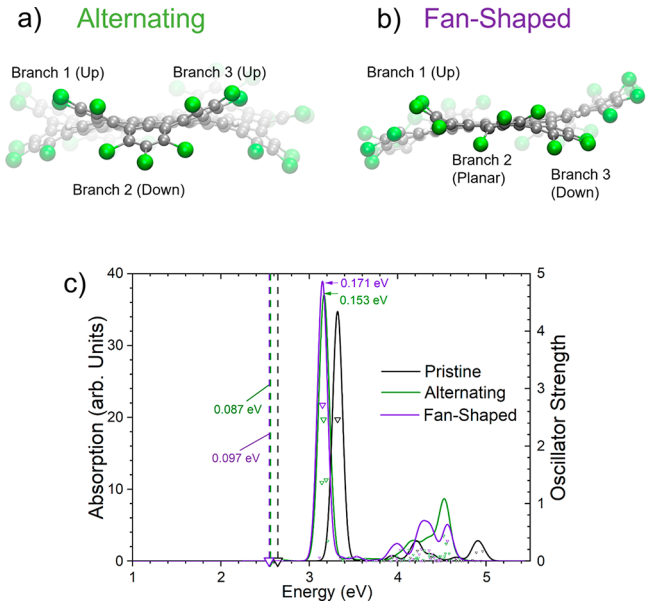

Figure 4. Alternating (a) and fan-shaped (b) conformers of the $C_{96}T$-27Cl GQD. These structures in their relaxed geometries show marked differences in their edge orientations. The alternating form has one planar branch, whereas the fan-shaped form contains a planar branch on all three fan regions around the GQD. (c) Calculated absorption spectra of Cl-Fan and Cl-Alt conformers. The oscillator strengths of electronic transitions contributing significantly to the spectra are numbered alongside their respective data points.

constructed with three groups (denoted "lobes") of three "branches", as labeled in Figure 1a. Each branch deviates from a plane of the remaining sheet by a degree that is dependent on the steric hindrance between the neighboring branches. The distinct orientations of these branches give rise to two different plausible conformations which we refer to as "alternating" (Figure 4a) and "fan-shaped" (Figure 4b). As the chlorine atoms on the branches repel each other, the branches are

https://doi.org/10.1021/acs.jpcc.1c00537
J. Phys. Chem. C 2021, 125, 9244−9252

relaxed in opposite out-of-plane direction of one another with respect to the rest of the GQD. We denote this as the "fan" orientation, where chlorine atoms fall above the plane, one in the plane, and one below the plane for all three branches (Figure 4b). The other possible orientation puts each of the chlorine atoms in alternating positions (i.e., one above the plane, one below the plane, and the third above the plane, etc.). This configuration forces two adjacent branches to both have the same orientation. As a result, the third branch must be in the "fan" configuration to avoid adjacent carbon atoms both in the "up" or "down" position (i.e., a geometrically frustrated structure). That branch acts as a transition point between up and down, with the middle group of the branch remaining planar (Figure 4b, branch 2).

In contrast to C_{96}T-3Cl, both conformations of the fully chlorinated C_{96}T GQD (C_{96}T-27Cl) are markedly nonplanar, and hence the excited state orbital distribution is heavily affected. While the fan-shaped dark state exciton (S_1) shows nearly full delocalization across the span of the GQD (Figure 3), the bright state (S_3) is very narrowly localized within a single lobe. The S_3 excitation is somewhat delocalized across the center of the structure. This behavior is similar in the alternating conformation to that of the fan-shaped conformation. The alternating dark state (S_1) shows delocalization in a similar manner to the fan-shaped dark state. However, the span is somewhat smaller, and in the bright state (S_3) the hole is extremely constrained to the single lobe that has a fanlike geometry. This demonstrates the localization of the excitation for both bright and dark states impacting the experimental emission energies.

The transition energies for these conformations compared to the pristine C_{96}T are shown in Figure 4c. The addition of 27 total chlorine atoms on the GQD edges results in a red-shift of the main absorption line from 3.3 eV in the pristine system to 3.18 eV in the alternating conformation. Change of the conformation to fan-shaped results in a stronger red-shift—as large as 2.95 eV for the main absorption line. These differences in the red-shift are attributed to increased exciton localization on planar regions of the structure. Fan-shaped branches deviate more from the planarity than alternating branches because the center functionalized atom is in the plane (forcing the atoms either side further out of plane). Because the alternating conformation possesses a single fan-shaped branch, the density delocalizes more easily in regions where the π-orbital overlap is large on the other branches. In fan-shaped system, there are three less-planar regions, one for each symmetrical domain of the GQD. Because the number of less-planar regions has increased compared to the alternating structure, the electrons tend to delocalize less. Ultimately we observe a stronger localization around the defect and a red-shift in the low-lying bright states in the absorption spectra (Figure 4c).

Because graphene flakes are typically studied in a dispersed solution, we further investigate the effects of solvation (see the Computational Methodology section) on the optical features of these structures. Overall, the aforementioned effects are qualitatively similar in the presence of solvent with solvatochromic red-shifts in optical spectra becoming more pronounced for high defect concentrations. For example, the effect of solvent on the optical transition energies of the C_{96}T GQD is shown in Figure 5. Comparing the fan conformation in vacuo to the solvated systems shows a solvatochromic red-shift of up to 120 meV for aniline/chlorobenzene. We additionally observe an increase in oscillator strength for the lower excited

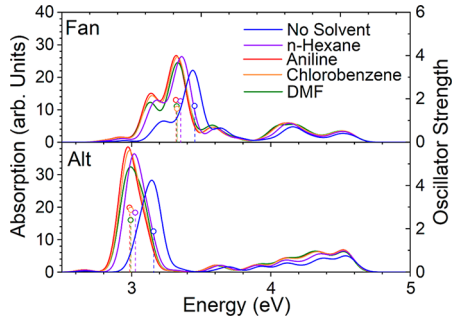

Figure 5. Calculated absorption spectra of alternating (top) and fan-shaped (bottom) conformers of the C_{96}T-27Cl GQD in various solvent environments. The oscillator strengths of brightest electronic transitions are indicated by sticks.

states of both solvated GQDs. This extent of solvatochromism is consistent with solvent effects reported in carbon quantum dots (CQDs).[29]

CONCLUSIONS

Our computational study shows that edge and corner chemical functionalization of graphene quantum dots leads to noticeable red-shifts in their electronic spectra and potentially enables tuning of their optical properties. Surprisingly, the origin of observed spectral changes is only weakly correlated to electron-donating/withdrawing capacity of substituents and is predominantly defined by substitution-induced deviations of the planar structure of graphene flakes. While monofunctionalization with strong electron-withdrawing groups introduces exciton localization on the GQD and creates a red-shift in optical spectra, this red-shift falls short of the magnitude induced by functionalization with less electron-withdrawing groups as observed in experiment. This indicates that further factors are involved in the red-shifting of the emission. In particular, functionalization of the edges of GQDs tends to break the molecular symmetry and the doubly degenerate excited states in the pristine form evolve into two lower lying bright states in certain functionalized structures. Significant effects on both the energy of the main absorption line and the ratio of oscillator strengths are observed, and the most red-shifted emission features are effectively enhanced. Functionalizing two or three sites results in the stronger red-shifts (especially for groups possessing strongly electron-withdrawing groups). However, as with monofunctionalization, these red-shifts fall short of those observed in experiment. In contrast, complete functionalization with chlorine atoms across all edges and corners reaches spectral shifts qualitatively similar to those observed in experiment, particularly in the presence of dielectric environments. This completely functionalized form results in a nonplanar buckled structure with two distinct and stable conformations, each bringing its own optical features as evidenced by orbital analysis of excited state spatial distribution. The optical features become red-shifted mostly due to the disruption from planarity.

This study attributes the predominant spectral red-shifts in functionalized GQDs to changes in geometry of the planar backbone, suggesting this as a useful route for tuning the optical energies in such materials. Overall, the versatility of the GQDs opens a wide possibility of future research avenues. For example, selective edge/corner functionalization may be combined with structures of specific topologies/geometries (such as square-shaped quantum dots). This may lead to an

https://doi.org/10.1021/acs.jpcc.1c00537
J. Phys. Chem. C 2021, 125, 9244−9252

interesting interplay of and coexistence of exited states with specific properties controlled by electronic localization.[30,31] Additionally, control over the degree of nonplanarity induced in these graphene systems shows promise for further tuning of optical properties and warrants further investigation into effects of strain.

COMPUTATIONAL METHODOLOGY

Ground-state optimal geometries and subsequent energies of emissive states were simulated by using DFT[32] and time-dependent DFT (TD-DFT)[33−37] approaches paired with a 6-31G basis set, respectively, as implemented in the Gaussian 16 by using the default convergence criteria of the software package.[38,39] In particular, in the case of geometry optimization, the RMS force criterion is set to 3.0×10^{-4} in atomic units. A proper choice of DFT model is critical for considered planar and near-planar GQDs, where an extended π-system enables edge-to-edge electronic delocalization. A well-studied small molecule coronene (Cn, $C_{24}H_{12}$) is a representative of these systems by exhibiting semiconducting electronic properties similar to that of GQDs. As such, it was selected as a reference structure with experimental data used for tuning our computational methodology. Here, ground and excited state calculations were performed by using several functionals including B3LYP, CAM-B3LYP, wB97X, and wB97XD models[40−43] to compare their relative accuracy with respect to the reference aiming to select the most promising method (see Figure S9). B3LYP is a common model which typically performs well on small molecular systems.[44] However, for these larger systems with extended electronic delocalization and a higher contribution from long-range interactions, it severely underestimates the bandgap. As expected, the other three range-separated hybrid functionals show better performance because of a more physical representation of exchange for long- and short-range interactions. Overall the CAM-B3LYP functional has demonstrated superior agreement with experimental data in calculation of bandgaps. While CAM-B3LYP was therefore chosen for all calculations presented, we expect similar qualitative description of electronic structure when using any range-separated DFT model. Modeling the optical properties of such large systems with reduced computational expense is possible by using semiempirical Hamiltonian models such as ZINDO/S. Our tests show trends similar to TDDFT by using such methods for select systems (Figure S10).

Functionalization of GQD edges with polar groups suggests exploration of dielectric medium effects. Solvation of the GQDs studied was simulated by using the polarizable continuum approach; specifically we used the Solvation Model based on Density (SMD) implemented in Gaussian 16.[38] The solvatochromic behavior was modeled in five solvents for selected structures, including *N*,*N*-dimethylformamide (DMF), chlorobenzene (CB), water, *n*-hexane, and aniline solvents. These were chosen as they are similar to commonly found graphene dispersions in the literature.[45−49] For computational efficiency, single point energies in SMD solvation shells[50] were calculated by using the structures optimized in the gas phase. Finally, the nature of the excited states for functionalized systems and their pristine counterparts was analyzed and compared at the TD-DFT level. Here electronic delocalization was tracked by using natural transition orbitals (NTOs) determined with Gaussian 16.[51,52] Figure S11 contains a table of oscillator strengths and energies for all systems in this study. Overall, the chosen methodology retains quantitative accuracy to the chosen experimental data and remains physically relevant to the phenomena we wish to describe as the range-corrected functional properly accounts for electronic delocalization in these confined graphene systems.

ASSOCIATED CONTENT

Supporting Information

The Supporting Information is available free of charge at https://pubs.acs.org/doi/10.1021/acs.jpcc.1c00537.

Figures S1−S11 (PDF)

AUTHOR INFORMATION

Corresponding Author

Alan Bishop − *Theoretical Division, Center for Nonlinear Studies (CNLS), and Center for Integrated Nanotechnologies (CINT), Los Alamos National Laboratory, Los Alamos, New Mexico 87545, United States*; Email: arb@lanl.gov

Authors

Andrew Sheely − *Theoretical Division, Center for Nonlinear Studies (CNLS), and Center for Integrated Nanotechnologies (CINT), Los Alamos National Laboratory, Los Alamos, New Mexico 87545, United States; NanoScience Technology Center, University of Central Florida, Orlando, Florida 32826, United States*

Brendan Gifford − *Theoretical Division, Center for Nonlinear Studies (CNLS), and Center for Integrated Nanotechnologies (CINT), Los Alamos National Laboratory, Los Alamos, New Mexico 87545, United States*; orcid.org/0000-0002-4116-711X

Sergei Tretiak − *Theoretical Division, Center for Nonlinear Studies (CNLS), and Center for Integrated Nanotechnologies (CINT), Los Alamos National Laboratory, Los Alamos, New Mexico 87545, United States*; orcid.org/0000-0001-5547-3647

Complete contact information is available at: https://pubs.acs.org/10.1021/acs.jpcc.1c00537

Notes

The authors declare no competing financial interest.

ACKNOWLEDGMENTS

The work at Los Alamos National Laboratory (LANL) was supported by the LANL Directed Research and Development Funds (LDRD) and performed in part at the Center for Nonlinear Studies (CNLS) and the Center for Integrated Nanotechnologies (CINT), a U.S. Department of Energy, Office of Science user facility at LANL. This research used resources provided by the LANL Institutional Computing (IC) Program. LANL is operated by Triad National Security, LLC, for the National Nuclear Security Administration of the U.S. Department of Energy (Contract 89233218NCA000001).

REFERENCES

(1) Novoselov, K. S.; Geim, A. K.; Morozov, S. V.; Jiang, D.; Zhang, Y.; Dubonos, S. V.; Grigorieva, I. V.; Firsov, A. A. J. s. Electric field effect in atomically thin carbon films. *Science* **2004**, *306*, 666−669.

(2) Craciun, M. F.; Russo, S.; Yamamoto, M.; Oostinga, J. B.; Morpurgo, A. F.; Tarucha, S. Trilayer graphene is a semimetal with a gate-tunable band overlap. *Nat. Nanotechnol.* **2009**, *4*, 383−388.

(3) Hernández Rosas, J. J.; Ramírez Gutiérrez, R. E.; Escobedo-Morales, A.; Chigo Anota, E. First principles calculations of the electronic and chemical properties of graphene, graphane, and graphene oxide. *J. Mol. Model.* **2011**, *17*, 1133−1139.
(4) Recher, P.; Trauzettel, B. Quantum dots and spin qubits in graphene. *Nanotechnology* **2010**, *21*, 302001.
(5) Novoselov, K. S.; Geim, A. J. N. M. The rise of graphene. *Nat. Mater.* **2007**, *6*, 183−191.
(6) Bacon, M.; Bradley, S. J.; Nann, T. Graphene Quantum Dots. *Part. Part. Syst. Charact.* **2014**, *31*, 415−428.
(7) Kovalchuk, A.; Huang, K.; Xiang, C.; Martí, A. A.; Tour, J. M. Luminescent Polymer Composite Films Containing Coal-Derived Graphene Quantum Dots. *ACS Appl. Mater. Interfaces* **2015**, *7*, 26063−26068.
(8) Moreno, C.; Vilas-Varela, M.; Kretz, B.; Garcia-Lekue, A.; Costache, M. V.; Paradinas, M.; Panighel, M.; Ceballos, G.; Valenzuela, S. O.; Peña, D.; et al. Bottom-up synthesis of multifunctional nanoporous graphene. *Science* **2018**, *360*, 199−203.
(9) Zhang, Y.; Tang, T.-T.; Girit, C.; Hao, Z.; Martin, M. C.; Zettl, A.; Crommie, M. F.; Shen, Y. R.; Wang, F. Direct observation of a widely tunable bandgap in bilayer graphene. *Nature* **2009**, *459*, 820−823.
(10) Georgakilas, V.; Otyepka, M.; Bourlinos, A. B.; Chandra, V.; Kim, N.; Kemp, K. C.; Hobza, P.; Zboril, R.; Kim, K. S. Functionalization of Graphene: Covalent and Non-Covalent Approaches, Derivatives and Applications. *Chem. Rev.* **2012**, *112*, 6156−6214.
(11) Meier, E.; An, F.; Gadway, B. Observation of the topological soliton state in the Su-Schrieffer-Heeger model. *Nat. Commun.* **2016**, *7*, 13986.
(12) Chen, S.; Zhao, Y.; Ullah, N.; Wan, Q.; Zhang, R. Revealing the trap emission in graphene-based nanostructures. *Carbon* **2019**, *150*, 439−445.
(13) Hu, Y.; Xie, P.; De Corato, M.; Ruini, A.; Zhao, S.; Meggendorfer, F.; Straasø, L. A.; Rondin, L.; Simon, P.; Li, J.; et al. Bandgap Engineering of Graphene Nanoribbons by Control over Structural Distortion. *J. Am. Chem. Soc.* **2018**, *140*, 7803−7809.
(14) Zheng, X. H.; Huang, L. F.; Wang, X. L.; Lan, J.; Zeng, Z. Band gap engineering in armchair-edged graphene nanoribbons by edge dihydrogenation. *Comput. Mater. Sci.* **2012**, *62*, 93−98.
(15) Tetsuka, H.; Asahi, R.; Nagoya, A.; Okamoto, K.; Tajima, I.; Ohta, R.; Okamoto, A. Optically Tunable Amino-Functionalized Graphene Quantum Dots. *Adv. Mater.* **2012**, *24*, 5333−5338.
(16) Sandeep Kumar, G.; Roy, R.; Sen, D.; Ghorai, U. K.; Thapa, R.; Mazumder, N.; Saha, S.; Chattopadhyay, K. K. Amino-functionalized graphene quantum dots: origin of tunable heterogeneous photoluminescence. *Nanoscale* **2014**, *6*, 3384−3391.
(17) Sekiya, R.; Uemura, Y.; Murakami, H.; Haino, T. White-Light-Emitting Edge-Functionalized Graphene Quantum Dots. *Angew. Chem., Int. Ed.* **2014**, *53*, 5619−5623.
(18) Zhao, S.; Lavie, J.; Rondin, L.; Orcin-Chaix, L.; Diederichs, C.; Roussignol, P.; Chassagneux, Y.; Voisin, C.; Mullen, K.; Narita, A.; Campidelli, S.; Lauret, J.-S. Single photon emission from graphene quantum dots at room temperature. *Nat. Commun.* **2018**, *9*, 3470.
(19) Li, X.; Lau, S. P.; Tang, L.; Ji, R.; Yang, P. Multicolour light emission from chlorine-doped graphene quantum dots. *J. Mater. Chem. C* **2013**, *1*, 7308−7313.
(20) Sharma, A.; Gifford, B. J.; Kilina, S. Tip Functionalization of Finite Single-Walled Carbon Nanotubes and Its Impact on the Ground and Excited State Electronic Structure. *J. Phys. Chem. C* **2017**, *121*, 8601−8612.
(21) Banerjee, S.; Bhattacharyya, D. Electronic properties of nanographene sheets calculated using quantum chemical DFT. *Comput. Mater. Sci.* **2008**, *44*, 41−45.
(22) Li, Y.; Shu, H.; Niu, X.; Wang, J. Electronic and Optical Properties of Edge-Functionalized Graphene Quantum Dots and the Underlying Mechanism. *J. Phys. Chem. C* **2015**, *119*, 24950−24957.
(23) Mombrú, D.; Romero, M.; Faccio, R.; Mombrú, Á. W. Electronic Structure of Edge-Modified Graphene Quantum Dots Interacting with Polyaniline: Vibrational and Optical Properties. *J. Phys. Chem. C* **2017**, *121*, 16576−16583.
(24) Feng, J.; Dong, H.; Yu, L.; Dong, L. The optical and electronic properties of graphene quantum dots with oxygen-containing groups: a density functional theory study. *J. Mater. Chem. C* **2017**, *5*, 5984−5993.
(25) Feng, J.; Dong, H.; Pang, B.; Shao, F.; Zhang, C.; Yu, L.; Dong, L. Theoretical study on the optical and electronic properties of graphene quantum dots doped with heteroatoms. *Phys. Chem. Chem. Phys.* **2018**, *20*, 15244−15252.
(26) Abdelsalam, H.; Elhaes, H.; Ibrahim, M. A. Tuning electronic properties in graphene quantum dots by chemical functionalization: Density functional theory calculations. *Chem. Phys. Lett.* **2018**, *695*, 138−148.
(27) Tan, Y.-Z.; Yang, B.; Parvez, K.; Narita, A.; Osella, S.; Beljonne, D.; Feng, X.; Müllen, K. Atomically precise edge chlorination of nanographenes and its application in graphene nanoribbons. *Nat. Commun.* **2013**, *4*, 2646.
(28) Yuan, F.; Yuan, T.; Sui, L.; Wang, Z.; Xi, Z.; Li, Y.; Li, X.; Fan, L.; Tan, Z.'a.; Chen, A.; Jin, M.; Yang, S. Engineering triangular carbon quantum dots with unprecedented narrow bandwidth emission for multicolored LEDs. *Nat. Commun.* **2018**, *9*, 2249.
(29) Pramanik, A.; Biswas, S.; Kumbhakar, P. Solvatochromism in highly luminescent environmental friendly carbon quantum dots for sensing applications: Conversion of bio-waste into bio-asset. *Spectrochim. Acta, Part A* **2018**, *191*, 498−512.
(30) Jaskólski, W.; Sarbicki, G. Topologically protected gap states and resonances in gated trilayer graphene. *Phys. Rev. B: Condens. Matter Mater. Phys.* **2020**, *102*, No. 035424.
(31) Yao, Q.; Chen, X.; van Bremen, R.; Sotthewes, K.; Zandvliet, H. J. W. Singularities and topologically protected states in twisted bilayer graphene. *Appl. Phys. Lett.* **2020**, *116*, No. 011602.
(32) Kohn, W.; Sham, L. J. Self-Consistent Equations Including Exchange and Correlation Effects. *Phys. Rev.* **1965**, *140*, A1133−A1138.
(33) Bauernschmitt, R.; Ahlrichs, R. Treatment of electronic excitations within the adiabatic approximation of time dependent density functional theory. *Chem. Phys. Lett.* **1996**, *256*, 454−464.
(34) Casida, M. E.; Jamorski, C.; Casida, K. C.; Salahub, D. R. Molecular excitation energies to high-lying bound states from time-dependent density-functional response theory: Characterization and correction of the time-dependent local density approximation ionization threshold. *J. Chem. Phys.* **1998**, *108*, 4439−4449.
(35) Stratmann, R. E.; Scuseria, G. E.; Frisch, M. J. An efficient implementation of time-dependent density-functional theory for the calculation of excitation energies of large molecules. *J. Chem. Phys.* **1998**, *109*, 8218−8224.
(36) Van Caillie, C.; Amos, R. D. Geometric derivatives of excitation energies using SCF and DFT. *Chem. Phys. Lett.* **1999**, *308*, 249−255.
(37) Trani, F.; Scalmani, G.; Zheng, G.; Carnimeo, I.; Frisch, M. J.; Barone, V. Time-Dependent Density Functional Tight Binding: New Formulation and Benchmark of Excited States. *J. Chem. Theory Comput.* **2011**, *7*, 3304−3313.
(38) Frisch, M. J.; Trucks, G. W.; Schlegel, H. B.; Scuseria, G. E.; Robb, M. A.; Cheeseman, J. R.; Scalmani, G.; Barone, V.; Petersson, G. A.; Nakatsuji, H.; et al. *Gaussian 16*, rev. C.01; Gaussian, Inc.: Wallingford, CT, 2016.
(39) Dennington, R.; Keith, T. A.; Millam, J. M. *GaussView*, ver. 5; Mission, KS, 2016.
(40) Becke, A. D. Density-functional thermochemistry. III. The role of exact exchange. *J. Chem. Phys.* **1993**, *98*, 5648−5652.
(41) Yanai, T.; Tew, D. P.; Handy, N. C. A new hybrid exchange−correlation functional using the Coulomb-attenuating method (CAM-B3LYP). *Chem. Phys. Lett.* **2004**, *393*, 51−57.
(42) Chai, J.-D.; Head-Gordon, M. Long-range corrected hybrid density functionals with damped atom−atom dispersion corrections. *Phys. Chem. Chem. Phys.* **2008**, *10*, 6615−6620.

https://doi.org/10.1021/acs.jpcc.1c00537
J. Phys. Chem. C 2021, 125, 9244−9252

(43) Krukau, A. V.; Vydrov, O. A.; Izmaylov, A. F.; Scuseria, G. E. Influence of the exchange screening parameter on the performance of screened hybrid functionals. *J. Chem. Phys.* **2006**, *125*, 224106.
(44) Tirado-Rives, J.; Jorgensen, W. L. Performance of B3LYP Density Functional Methods for a Large Set of Organic Molecules. *J. Chem. Theory Comput.* **2008**, *4*, 297−306.
(45) Burdett, J. J.; Müller, A. M.; Gosztola, D.; Bardeen, C. J. Excited state dynamics in solid and monomeric tetracene: The roles of superradiance and exciton fission. *J. Chem. Phys.* **2010**, *133*, 144506.
(46) Hesse, R.; Hofberger, W.; Bässler, H. Absorption spectra of disordered solid tetracene and pentacene. *Chem. Phys.* **1980**, *49*, 201−211.
(47) Hummer, K.; Ambrosch-Draxl, C. Electronic properties of oligoacenes from first principles. *Phys. Rev. B: Condens. Matter Mater. Phys.* **2005**, *72*, 205205.
(48) Jankowiak, R.; Rockwitz, K. D.; Baessler, H. Adsorption spectroscopy of amorphous tetracene. *J. Phys. Chem.* **1983**, *87*, 552−557.
(49) Yeh, C.-N.; Wu, C.; Su, H.; Chai, J.-D. Electronic properties of the coronene series from thermally-assisted-occupation density functional theory. *RSC Adv.* **2018**, *8*, 34350−34358.
(50) Marenich, A. V.; Cramer, C. J.; Truhlar, D. G. Universal Solvation Model Based on Solute Electron Density and on a Continuum Model of the Solvent Defined by the Bulk Dielectric Constant and Atomic Surface Tensions. *J. Phys. Chem. B* **2009**, *113*, 6378−6396.
(51) Martin, R. L. Natural transition orbitals. *J. Chem. Phys.* **2003**, *118*, 4775−4777.
(52) Tretiak, S.; Saxena, A.; Martin, R. L.; Bishop, A. R. Collective electronic oscillator/semiempirical calculations of static nonlinear polarizabilities in conjugated molecules. *J. Chem. Phys.* **2001**, *115*, 699−707.

https://doi.org/10.1021/acs.jpcc.1c00537
J. Phys. Chem. C 2021, 125, 9244−9252